

# Synthesis and characterization of CdS nanoparticles decorated TiO<sub>2</sub> matrix for an efficient N3 based dye sensitized solar cell (DSSC)

Sayantani Bhattacharya<sup>1</sup> · Arunava Pal<sup>1</sup> · Atanu Jana<sup>1</sup> · Jayati Datta<sup>1</sup>

Received: 29 December 2015 / Accepted: 1 July 2016 / Published online: 8 July 2016  
© Springer Science+Business Media New York 2016

**Abstract** The conventional dye sensitized solar cell (DSSC) comprise of mostly the titania matrix sensitized with absorber dye molecules acting as light energy scavengers. The present investigation deals with formulating CdS–TiO<sub>2</sub> conjugate matrix for the DSSC system using N3 dye sensitizer. TiO<sub>2</sub> nanoparticles (NPs) were pasted on FTO glass substrate and thin film of CdS was coated on titania matrix by chemical bath deposition technique using precursors cadmium acetate and thiourea. The differential absorbance spectra of the CdS–TiO<sub>2</sub> conjugate system shows sharp absorption edges around 345–500 nm, corresponding to band gap energies in the region 3.59 and 2.47 eV respectively, indicative of formation of two distinguishable energy region for the existence of the nano crystallites of both TiO<sub>2</sub> and CdS. The shift in Raman bands was also observed with the incorporation of CdS in TiO<sub>2</sub> matrix. XRD data confirms the formation of crystalline CdS nanoparticles. The FE–SEM images revealed that the TiO<sub>2</sub> particles are spherical and monodispersed having diameter in the range 20–30 nm and embedded with CdSNPs of average particle size 10–15 nm. The performance characteristics of the synthesized films towards photovoltaic behavior were studied with the record of short circuit currents through *J–V* measurement using N3 absorber dye and the I<sup>−</sup>/I<sub>3</sub><sup>−</sup> electrolyte under 30 mW cm<sup>−2</sup> light intensity. An effective increase of efficiency is observed with the CdS modified TiO<sub>2</sub> matrix compared to the bare TiO<sub>2</sub> in the DSSC system and a maximum photo-

conversion efficiency of 7.5 % was obtained with the optimized dye loading. Impedance spectroscopic measurements give important information about the interfacial electron injection and recombination dynamics of the device. The incident photon-to-current conversion efficiency measurements show that both the absorbers CdS and N3 dye, contribute to the cell performance.

## 1 Introduction

Dye-sensitized solar cell (DSSC) is an alternate solar cell technology to the thin film photovoltaic systems based on thin layers of various low and moderate band gap semiconductor materials such as amorphous silicon, cadmium telluride (CdTe), copper indium gallium diselenide and many other chalcogenides [1–5]. Even though the thin film solar cell requires less material, the complex production processes of the different combinations of the rare materials are expensive and may limit the future large-scale production. It may be understood that the large band gap TiO<sub>2</sub> (3.2 eV) itself, limits its absorption to the ultraviolet region of the solar spectrum and also lack in electron mobility between the energy states, however, with the sensitizer dye it performs well in the DSSC system [6, 7]. Typical DSSCs consist of a wide band gap semiconductor matrix, frequently used titanium dioxide (TiO<sub>2</sub>), onto which sensitizer dye molecules are attached acting as light absorbers [8–11]. The charge separation takes place at the interface via photo induced electron injection from the dye into the conduction band of the TiO<sub>2</sub> and further to the charge collector. Eventually the dye is restored in its original form by electron donation from I<sub>3</sub><sup>−</sup>/I<sup>−</sup> acting as the electrolyte.

In order to enhance the light harvesting phenomenon in the visible region, several efforts have been made on the

✉ Jayati Datta  
jayati\_datta@rediffmail.com

<sup>1</sup> Department of Chemistry, Indian Institute of Engineering Science and Technology, Shibpur, Howrah, West Bengal 711 103, India

development of energy efficient sensitizers including inorganic and organic dyes, quantum dots, plasmonic nanoparticles etc. [12–14]. Several reports are available on DSSC systems using standard dyes like N3, N719, black dye (N749) etc. [15–17]. Eosin Y has emerged as an effective metal free organic sensitizer dye for DSSC system [18]. Further, coumarine/polyene type sensitizers have been reported to exhibit 7.7 % efficiency in DSSC system [19, 20]. The semiconductors such as CdS, CdSe, CdTe, PbS, Bi<sub>2</sub>S<sub>3</sub>, CuInS<sub>2</sub> can also serve as effective sensitizers as they absorb visible light and are able to inject the excited electrons to the conduction band of TiO<sub>2</sub> [21–25]. The CdS NPs have been chosen as an additional sensitizer attached to the TiO<sub>2</sub> matrix in the present study and is expected to excite electrons easily from its valance band to conduction band (CB). Further since the Cd-chalcogenide resides at higher energy state than the TiO<sub>2</sub> CB, electron injection rapidly takes place from the energy bands of CdS to that of TiO<sub>2</sub>. Moreover, amongst the Cd chalcogenide family, CdS can firmly resist photo-dissolution and thereby lead to high life span of the photo electrode as shown in one of our earlier works on liquid junction solar cell [26]. From the above stand point, the authors attempt to fabricate a conjugate structure photoanode consisting of a sensitizing Cd-chalcogenide layer coated on the wide band gap TiO<sub>2</sub> matrix and subsequently sensitizing the composite matrix with absorber N3 dye molecules. The multi faceted functional properties of the composite make the chalcogenide–dye coupled DSSC a more efficient and stable photon to current conversion device compared to the typical TiO<sub>2</sub> based DSSC [16, 27, 28].

## 2 Experimental

### 2.1 Synthesis of TiO<sub>2</sub> NPs

TiO<sub>2</sub> nanoparticles (NPs) have been prepared by using a solution of 1.5 M Ammonium perdisulphate and 0.75 M Titanium (IV) Chloride. The aqueous solution was heated at 75 °C and maintained at the same temperature for 90 min. Subsequently, 2.5 M Ammonium hydroxide solution was added drop wise under high speed stirring until the pH reached to seven. The precipitated titanium hydroxide was collected, repeatedly washed with aqueous ethanol followed by drying at 50–55 °C to obtained TiO<sub>2</sub>NPs.

### 2.2 Preparation of CdS–TiO<sub>2</sub> photo-anode

The laboratory prepared anatase TiO<sub>2</sub> were mixed with commercially available Degussa P25 (TiO<sub>2</sub>) (Sigma Aldrich) in 2:3 proportion in ethanolic solution containing acetic acid, ethyl cellulose and terpineol (Fluka) as the

binding agents. The TiO<sub>2</sub> paste was ultra-sonicated to maintain the homogeneity of the solution and further concentrated by evaporation. In course of fabrication of the DSSC anode, TiO<sub>2</sub> paste was uniformly coated on FTO glass substrate (Dyesol, Australia) by the help of doctor's blade technique and sintered at 500 °C for 30 min. The TiO<sub>2</sub> thin films were cooled to room temperature for further modification [29].

CdS layers were deposited onto TiO<sub>2</sub> thin film substrates by the chemical bath deposition technique. The titania films were immersed into 0.005 M cadmium acetate solution at bath temperature of 85 °C and 0.01 M of thiourea solution was added dropwise. The pH of the mixture was maintained at nine, and the solution turned yellow. The CdS–TiO<sub>2</sub> films obtained were washed thoroughly with deionised water and heated at around 90 °C for 10 min.

### 2.3 Dye sensitized solar cell assembly

The bare TiO<sub>2</sub> and the CdS–TiO<sub>2</sub> films coated on FTO glass substrate were sensitized overnight with 1 mM ethanolic solution of N3 ([RuL<sub>2</sub>(NCS)<sub>2</sub>·2H<sub>2</sub>O; L = 2,2'-bipyridine-4,4'-dicarboxylic acid) dye. The cathode was fabricated by electrodeposition (galvanostatic) of Pt NPs onto FTO glass from 1 mM H<sub>2</sub>PtCl<sub>6</sub> (Arora Matthey, India) in H<sub>2</sub>SO<sub>4</sub> solution under current density of 5 mA cm<sup>-2</sup> by the help of electrochemistry work station AUTOLAB 302 N, Metrohm B.V. (The Netherlands). The anode and the cathode were assembled using Bynel (SX1170-60, 50 μm thick, Solaronix) as the sealant and heating at ~80 °C. The working electrolyte consisting of 0.05 M triphenylmethylphosphonium iodide (TPMPI), 0.5 M sodium iodide, 0.05 M iodine, and 0.5 M 4-tertbutyl pyridine (TBP) (Sigma-Aldrich) in acetonitrile was subsequently injected into the cell. TBP acted as a binder molecule for the dye and the electrolytic species to the nano-porous TiO<sub>2</sub> matrix. The active area of the electrode was limited to 0.5 cm<sup>2</sup> by the sealing frame.

### 2.4 UV–Vis and Raman spectroscopy

The absorbance of the as prepared pure TiO<sub>2</sub>NPs, pure CdS, and CdS–TiO<sub>2</sub> conjugate systems were obtained within the spectral range 300–800 nm as recorded in JASCO V-530 UV–VIS–NIR Spectrophotometer, Japan. The films matrix were further analyzed through FT-Raman spectroscopy within the Raman shift range of 100–800 cm<sup>-1</sup> using Spex double monochromator (model 1403) fitted with a holo graphic grating of 1800 grooves/mm and a cooled photomultiplier tube (model R928/115) from Hamamatsu Photonics, Japan, excited with 514.5 nm radiation from a Spectra Physics Ar<sup>+</sup> ion laser (model 2020-05) at 200 mW power with acquisition time 0.5 s.

## 2.5 SEM, EDAX and XRD analysis

The synthesized films were subjected to morphological and compositional analysis through SEM in a JEOL JSM-6700F FESEM coupled with EDAX analyzer using Oxford X-ray detector. The crystallinity of the surface was studied by employing Philips PW 1710, X-ray diffractometer using  $\text{CuK}\alpha$  radiation of wavelength  $1.542 \text{ \AA}$  and operated on 25 kV, 20 mA within the  $2\theta$  ranging between  $20^\circ$  and  $80^\circ$ .

## 2.6 Variation of dye loading and current density–voltage plot

The concentration of the N3 dye solution in ethanol was varied in the range  $10^{-5} \text{ (M)}\text{--}10^{-1} \text{ (M)}$ . The cell system  $\text{FTO}\text{--}\text{CdS}\text{--}\text{TiO}_2\text{--}\text{N3}/\text{electrolyte}/\text{Pt}\text{--}\text{FTO}$  was subjected to current density–voltage measurement at various dye concentrations as mentioned above, by the help of AUTOLAB 302 N, Metrohm Autolab B.V. (The Netherlands) combined with NOVA-v1.10 software package under  $30 \text{ mW cm}^{-2}$  illumination with white LED light source.

## 2.7 Electrochemical impedance spectroscopy (EIS)

The  $\text{TiO}_2\text{--}\text{CdS}/\text{dye}/\text{electrolyte}$  interface of the fabricated DSSC was subjected to the study of electrochemical impedance spectroscopy (EIS) taking the optimized loading of the dye, to reveal the interfacial characteristics in terms of electrical and electrochemical parameters of the solar cell in operation. Measurements were carried out with the same electrochemistry system as mentioned above under similar illumination condition by applying sinusoidal perturbation of 5 mV amplitude over a frequency range of 100 kHz–10 mHz at a respective bias open circuit potential ( $V_{oc}$ ).

## 2.8 Photovoltaic measurements of DSSC

The photovoltaic measurements, in terms of current–voltage  $J\text{--}V$  plots, were carried out in the DSSC set up using the dye loaded bare  $\text{TiO}_2$  and conjugated  $\text{CdS}\text{--}\text{TiO}_2$  matrices as well as using the  $\text{CdS}\text{--}\text{TiO}_2$  matrix without the dye attached to it. Incident photon to current conversion efficiency (% IPCE) was measured by using a monochromator with a 200 W xenon lamp power supply (9055 monochromator, Canada) connected with the same electrochemistry system.

## 2.9 Photo-voltage decay measurement

Photovoltage decay of the fabricated DSSC system using  $\text{N3}\text{--}\text{TiO}_2$  and  $\text{N3}\text{--}\text{CdS}\text{--}\text{TiO}_2$  matrices as photoanode were measured in terms of chrono-potentiometric analysis using similar electrochemical set up as mentioned earlier.

## 3 Results and discussion

### 3.1 Optical characterisation of the $\text{CdS}\text{--}\text{TiO}_2$ conjugate matrix

The absorbance spectra for the film regime are presented in Fig. 1. The differential absorbance spectra (Fig. 1 Inset) of  $\text{CdS}\text{--}\text{TiO}_2$  conjugate system shows sharp absorption edges around 345 and 500 nm, corresponding to band gap energies in the region 3.59 and 2.47 eV respectively, indicative of formation of two distinguishable energy region corresponding to the existence of both  $\text{TiO}_2$  and CdS NPs. Incorporation of CdS onto the titania matrix broadens the absorption nature of pure  $\text{TiO}_2$ . The distinct peaks in the visible region, confirmed the adsorption geometry and the feasibility of the employed model.

### 3.2 Raman study of $\text{CdS}\text{--}\text{TiO}_2$ matrix

The Raman spectral observations (Fig. 2) elucidate the variations in the Raman bands of  $\text{TiO}_2$  NPs and the shifting in energy due to incorporation of CdS in  $\text{TiO}_2$ . Considering mainly the anatase form of  $\text{TiO}_2$ , the character table of D4h point group shows anatase has six Raman active modes ( $A_{1g} + 2B_{1g} + 3E_g$ ) [30]. The typical peaks of the longitudinal optical (LO) modes, the fundamental frequency at  $300 \text{ cm}^{-1}$  (1LO) and the first overtone at  $600 \text{ cm}^{-1}$  (2LO) of CdS were observed from the spectra. From the Fig. 2, it is clear that for  $\text{CdS}\text{--}\text{TiO}_2$ , the peaks of only  $\text{TiO}_2$  arises at  $144 \text{ cm}^{-1}$  ( $E_g$ ),  $396 \text{ cm}^{-1}$  ( $B_{1g}$ ),  $513 \text{ cm}^{-1}$  ( $A_{1g}$ ) and  $639 \text{ cm}^{-1}$  ( $E_g$ ) [31] where as the peaks for CdS are observed at 300 and  $600 \text{ cm}^{-1}$  respectively [32]. The appreciable peak shifting (blue shift) from  $144$  to  $147.8 \text{ cm}^{-1}$  is therefore distinguishable after incorporation of CdS NPs in  $\text{TiO}_2$  matrix.

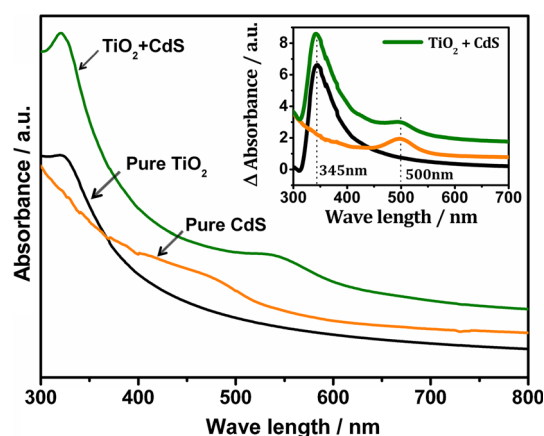


**Fig. 1** UV–Vis absorption spectra of Pure  $\text{TiO}_2$ , Pure CdS and  $\text{TiO}_2\text{--}\text{CdS}$  conjugate matrix. Inset shows corresponding differential absorbance spectra

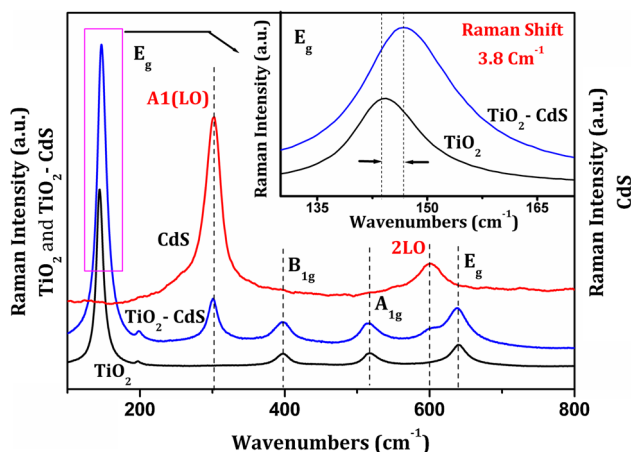


**Fig. 2** Raman spectra of TiO<sub>2</sub>, CdS and TiO<sub>2</sub>-CdS electrode by excitation at 514 nm

### 3.3 X-ray diffraction and morphology of the conjugate matrix

The typical FESEM images of TiO<sub>2</sub> NPs prepared in the laboratory are shown in Fig. 3a. The FE-SEM images revealed that the TiO<sub>2</sub> particles are spherical and monodispersed with a diameter of 20–30 nm. Figure 3c shows a typical SEM image of the CdS coated titania with a narrow size distribution with an average diameter of 10–15 nm, whereas pure CdS on FTO glass (Fig. 3b), consist of a compact layer of spherical CdS particles with

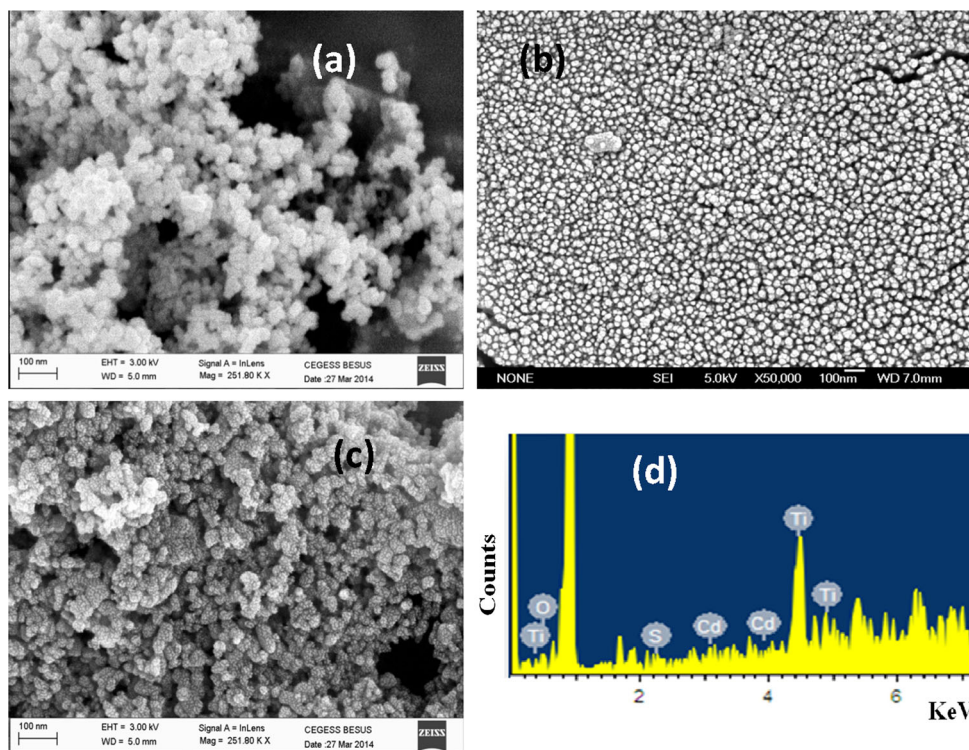
diameter 20–30 nm. The micrographs reveal homogeneous and compact nanocrystalline structure composed of spherically shaped well-defined grains. The EDAX study (Fig. 3d) reveals the presence of cadmium (Cd) and sulphide (S) as the elementary components along with titanium (Ti) and oxygen (O) in all the samples.

The TiO<sub>2</sub> and CdS–TiO<sub>2</sub> composites were also subjected to X-ray powder diffraction analysis. The XRD profile for TiO<sub>2</sub>, and CdS–TiO<sub>2</sub> samples are shown in Fig. 4. The peaks arises for anatase TiO<sub>2</sub> at 25°, 37.38°, 48°, 54°, 55° and 62.76° etc. and the corresponding *h, k, l* values for each of these peaks were indexed with the help of JCPDS data files (JCPDS: 21-1272; 43-0985) and shown in the Fig. 4 [33]. The Bragg’s ‘*d*’ value for the TiO<sub>2</sub> matrix was found to be 3.5 ± 0.1 Å, corresponding to [101] peak of anatase TiO<sub>2</sub> nano particles. However, CdS–TiO<sub>2</sub> composite shows typical diffraction patterns of orthorhombic structure of CdS at 2θ = 37° and 41.38°, corresponding to [101] and [111]. The average size of the TiO<sub>2</sub> particles were calculated by using the Scherrer equation [34] (considering the 101 plane) and lie in between 20 and 25 nm whereas CdS particles (considering the 111 plane) were found to be ~20 nm in size.

### 3.4 Electrochemical impedance spectroscopy (EIS)

The feasibility of charge transfer process across the photo anode–redox electrolyte interface was revealed through

**Fig. 3** SEM micrographs of **a** TiO<sub>2</sub> **b** Pure CdS on FTO **c** CdS–TiO<sub>2</sub> matrix on FTO and **d** EDAX for CdS–TiO<sub>2</sub> matrix



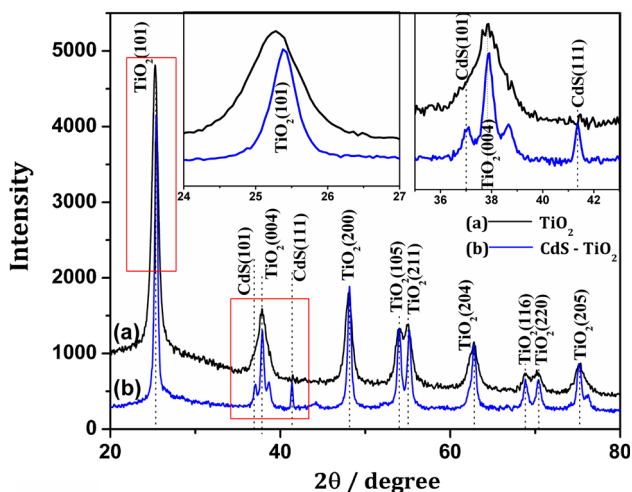


**Fig. 4** X-ray Diffraction pattern of *a* TiO<sub>2</sub> and *b* CdS–TiO<sub>2</sub> matrix

EIS measurements of the bare TiO<sub>2</sub> and composite CdS–TiO<sub>2</sub> matrix as manifested in the Nyquist plots (Fig. 5). The data were best fitted to the Randles equivalent circuit (*EC*) model (Fig. 5a inset) where the circuit included an ohmic resistance ( $R_h$ ), charge transfer resistance ( $R_{ct}$ ), constant phase element (*CPE*) as the non-ideal capacitor suggestive of the surface states and heterogeneous nature of the SC films [26] and the Warburg impedance (*W*) due to the ions diffused in the electrolyte. The Nyquist plot of the CdS–TiO<sub>2</sub> film is featured with two consecutive semicircles labelled as *R1* (5.3) and *R2* (39.1  $\Omega$ ) associated with the complex impedance of charge transfer at the CdS/electrolyte and TiO<sub>2</sub>/dye/electrolyte interface respectively. The DSSC with CdS–TiO<sub>2</sub> anode was found to

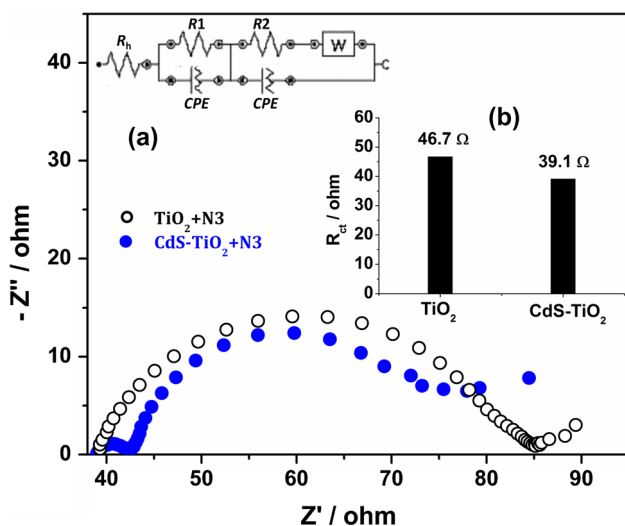


**Fig. 5** Nyquist plot of the N3–CdS–TiO<sub>2</sub> and N3–TiO<sub>2</sub> over a frequency range of 100 kHz–10 mHz; *Inset* shows *a* Equivalent circuit diagram *b* bar plot of  $R_{ct}$  variation with anode matrix

exhibit lower charge transfer resistance (39.1  $\Omega$ ) compared to that using pure TiO<sub>2</sub> (46.7  $\Omega$ ) (Fig. 5b) and significantly improved cell performance. This may be rationalized due to incorporation of low band gap CdS semiconductor which facilitates the ion transport across the electrode–electrolyte interface, thereby enhancing charge transfer kinetics of the DSSC reaction sequences.

### 3.5 Effect of TPMPI in the electrolyte

TPMPI is usually advocated for use as the electrolyte component in DSSC systems operable under low light conditions. It may be understood that the organic electrolyte added to the  $I^-/I_3^-$  system, imparts an overall stability to the interfacial region by suppressing the photo corrosion of the matrix. In case of using NaI in the electrolyte, Na<sup>+</sup> being a hard cation and small in size, strongly interacts with the negatively charged TiO<sub>2</sub> and penetrates within the dye adsorbed surface creating a pre-electrode layer of halide ions at the interface, whereas, the large organic cation MePh<sub>3</sub>P<sup>+</sup> gets involved in soft–soft interaction with the TiO<sub>2</sub>/dye structure with much less penetration power. TPMPI therefore functionalize the interfacial properties by extending the interfacial double-layer, thus indirectly reducing the local concentration of I<sub>3</sub><sup>−</sup> resulting in the longer lifetime of the system [35].

### 3.6 Photovoltaic performance and %IPCE analysis

The performance characteristics of the synthesized films towards photovoltaic behavior were studied, taking various concentrations of the N3 dye, in the cell configured as FTO–TiO<sub>2</sub>–CdS–dye/electrolyte/Pt–FTO with the record of short circuit currents ( $J_{sc}$ ) through *J–V* measurement. The *J–V* plots are shown in Fig. 6a where the inset corresponds to the *J–V* parameters profile. The best performance output is observed at a loading of 10<sup>−3</sup> (M) dye concentration. The power output characteristics of DSSC constituted with the N3–TiO<sub>2</sub>, N3–CdS–TiO<sub>2</sub> matrices, using the optimized dye loading are demonstrated in Fig. 6b, with simultaneous record of the open circuit voltage ( $V_{oc}$ ) and short circuit currents ( $J_{sc}$ ). The *J–V* parameters were also recorded for CdS–TiO<sub>2</sub> without using dye so as to compare with the dye loaded matrices. The values derived thereof are summarized in Table 1. There is an effective increase in efficiency for the CdS decorated TiO<sub>2</sub> matrix with the short circuit current remaining almost the same while the CdS–TiO<sub>2</sub> shows poor cell efficiency (0.49 %) without using the dye, however, substantial *FF* of 55.3 % is observed in the latter case. The efficiency of photo-conversion ( $\eta$ ) increases from 6.23 to 7.5 % while *FF* increases to the level of ~48 % for the N3–CdS–TiO<sub>2</sub> conjugate matrix compared to N3–TiO<sub>2</sub> matrix. The

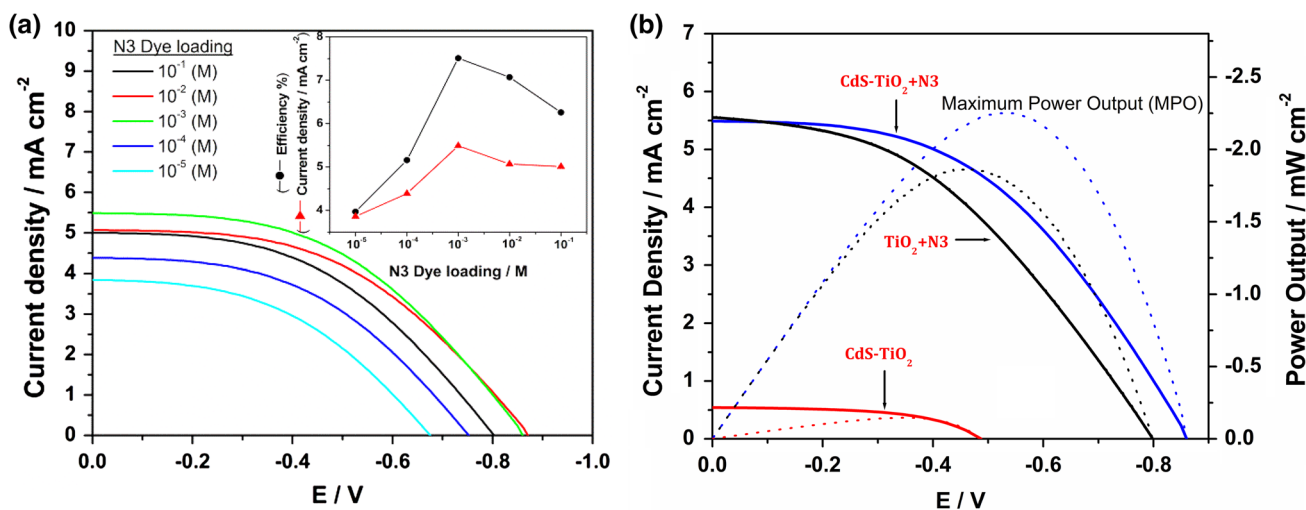


**Fig. 6** **a** *J*–*V* plot of the CdS–TiO<sub>2</sub> based DSSC for different N3 dye loading and in inset variation of efficiency and current density with dye concentration. **b** *J*–*V* curves (solid line) and power output plot

(dotted line) of the CdS–TiO<sub>2</sub>, N3–TiO<sub>2</sub>, and N3–CdS–TiO<sub>2</sub> based DSSC under light intensity 30 mW cm<sup>−2</sup>

**Table 1** Photovoltaic data for fabricated DSSC

PV parameters	Anode matrix for DSSC		
	CdS–TiO <sub>2</sub>	N3–TiO <sub>2</sub>	N3–CdS–TiO <sub>2</sub>
<i>J</i> <sub>sc</sub> (mA cm <sup>−2</sup> )	0.542	5.55	5.50
<i>V</i> <sub>oc</sub> (mV)	487	790	860
<i>η</i> %	0.49	6.23	7.50
<i>FF</i> %	55.30	42.25	47.65
MPO (mW cm <sup>−2</sup> )	0.146	1.857	2.225

additional CdS layer in the matrix, although not able to complete the DSSC phenomenon alone, accelerates the unidirectional transport of electrons in the TiO<sub>2</sub> film which reduces the recombination and increases the cell performance [36]. Therefore it is the conjugate effect of CdS and N3 that enables the proposed DSSC to harness energy more efficiently. The photovoltaic parameters %*η* and %*FF* are expressed by the following equations:

$$\% \eta = \frac{V_{max} \times J_{max}}{P_{in}} \times 100 \tag{1}$$

$$\% FF = \frac{V_{max} \times J_{max}}{V_{OC} \times J_{sc}} \times 100 \tag{2}$$

where, *P*<sub>in</sub>, input power, *V*<sub>max</sub> and *J*<sub>max</sub> are the voltage and current density respectively corresponding to the maximum output power, *V*<sub>oc</sub> and *J*<sub>sc</sub> are open circuit voltage and short circuit current density respectively [26].

The shunt and series resistances for fabricated DSSC system with bare TiO<sub>2</sub> and modified TiO<sub>2</sub> electrodes have been evaluated from the tangential slope of current–voltage

(*J*–*V*) plots at near *J*<sub>sc</sub> and near *V*<sub>oc</sub> regions, respectively [37]. It is observed that shunt resistance, *R*<sub>sh</sub> for the conjugate N3–CdS–TiO<sub>2</sub> system is much higher (1.87 KΩ) than that for the bare N3–TiO<sub>2</sub> system (0.6 KΩ), indicating sluggish back electron transfer kinetics between TiO<sub>2</sub>–dye at the dye–electrode/electrolyte interface, thus reducing the rate of recombination. On the other hand, the series resistance (*R*<sub>s</sub>) for the DSSC system decreases from 93.42 to 88.4 Ω with the introduction of smaller CdS NPs onto the TiO<sub>2</sub> matrix, due to increase of the electrode surface area and rapid charge–transfer kinetics at the interface.

The incident photon to current conversion efficiency (IPCE) spectrum is derived using the following equation [38]:

$$\% IPCE = \frac{1240 \times J_{sc}(A/cm^2)}{P(W/cm^2) \times \lambda(nm)} \times 100 \tag{3}$$

where *J*<sub>sc</sub> is the photocurrent density generated by monochromatic light specified by wavelength *λ* and power density *P*. The IPCE spectra of N3 sensitized TiO<sub>2</sub> and CdS–TiO<sub>2</sub> solar cells are shown in Fig. 7. There is an active participation of CdS throughout the spectral range of the visible light as observed in the IPCE pattern. The maximum IPCE reached 55 % for N3–TiO<sub>2</sub> system while 60 % is achieved for N3–CdS–TiO<sub>2</sub> based photoanode at 560 nm. Therefore the electron transfer kinetics from excited CdS and N3 to the conduction band of TiO<sub>2</sub> is more facile for the CdS–TiO<sub>2</sub> conjugate structure.

### 3.7 Photo-voltage decay

The time dependent variation of photo-voltage (Fig. 8) was conducted for 2 h with the DSSC system. The conjugate

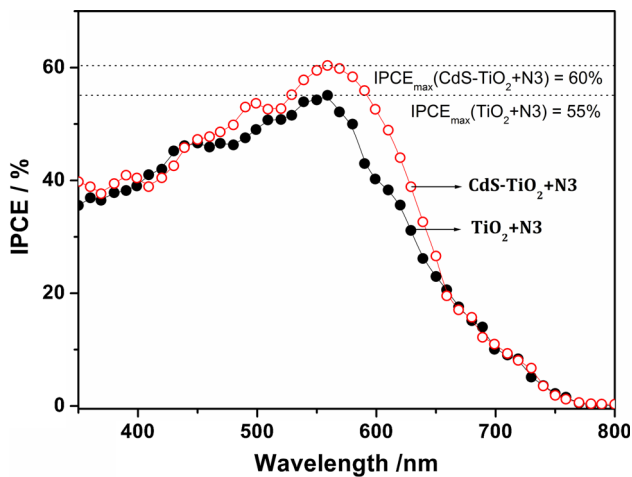


**Fig. 7** IPCE spectra as a function of wavelength for the N3-sensitized and N3-CdS sensitized TiO<sub>2</sub> solar cell

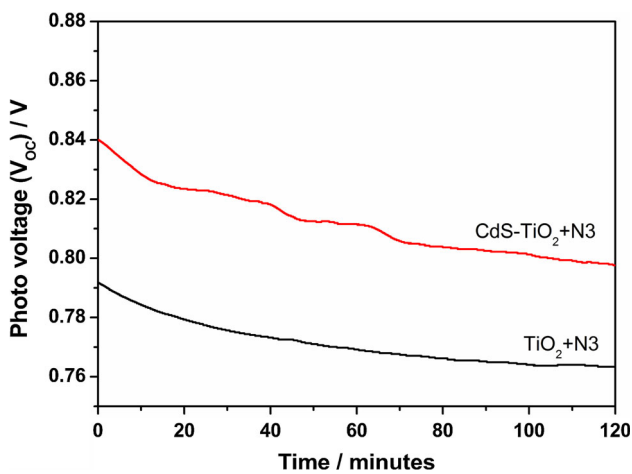


**Fig. 8** Photo-voltage decay with time for TiO<sub>2</sub> and CdS-TiO<sub>2</sub> in N3 dye system

system (CdS-TiO<sub>2</sub>) showed considerable stability and the degradation is almost three times for bare TiO<sub>2</sub> compared to the CdS-TiO<sub>2</sub> matrix. The decay ( $\delta$ ) is calculated from the photo voltage-time profile using the following relation [39],

$$\delta \% = \frac{100}{v_o} \times \frac{dv}{dt} \quad (4)$$

where  $v_o$  is the initial potential obtained from back extrapolation of the linear potential decay and  $t$  is the time in minutes.

## 4 Conclusion

In the present investigation we have demonstrated the beneficial effect of using the lower energy CdS NPs as sensitizer film along with the absorber N3 dye, for tuning

the optical path length of TiO<sub>2</sub>NPs. CdS-TiO<sub>2</sub> composite matrix shows two distinct band gap energies at 3.59 and 2.47 eV for TiO<sub>2</sub> and CdS respectively. XRD analysis confirms the presence of orthorhombic CdS structure in the CdS-TiO<sub>2</sub> composite matrix. The power output characteristics of the cell system comprised of the N3-CdS-TiO<sub>2</sub> as the anode at an optimum dye loading shows maximum photo conversion efficiency of 7.50 % and  $FF$  of 48 % under white LED light source. It is therefore evident that TiO<sub>2</sub> with the coupled sensitizer CdS and N3 dye widens the spectral response, promotes the photon to current conversion, arrests the interfacial charge recombination and ultimately increases the efficacies of the DSSC in harvesting light from the visible spectrum.

**Acknowledgments** The authors gratefully acknowledge Department of Science and Technology (DST-SERI) for financial support and MHRD, New Delhi, Govt. of India for the instrumental facilities provided to the Department. S. Bhattacharya thanks UGC, New Delhi for providing Junior Research Fellowship.

## References

1. B. O'Regan, M. Gratzel, *Nature* **353**, 737 (1991)
2. Z. Lan, J. Wu, J. Lin, M. Huang, *J. Mater. Sci. Mater. Electron.* **21**, 833 (2010)
3. B. Liu, R. Luo, Q. Liang, Y. Zheng, B. Li, J. Zhang, W. Li, L. Wu, L. Feng, *J. Mater. Sci. Mater. Electron.* **26**, 9985 (2015)
4. H. Movla, A.M. Rafi, N.M. Rafi, *Optik* **126**, 5088 (2015)
5. S. Sharbati, S.H. Keshmiri, J.T. McGoffin, R. Geisthardt, *Appl. Phys. A* **118**, 1259 (2015)
6. P.E. De Jongh, D. Vanmaekelbergh, *Phys. Rev. Lett.* **77**, 3427 (1996)
7. G. Schlichthorl, S.Y. Huang, J. Sprague, A.J. Frank, *J. Phys. Chem. B* **101**, 8141 (1997)
8. N. Tétreault, É. Arsenault, L.P. Heiniger, N. Soheilnia, J. Brillet, T. Moehl, S. Zakeeruddin, G.A. Ozin, M. Grätzel, *Nano Lett.* **11**, 4579 (2011)
9. L. Kavan, J.H. Yum, M. Gratzel, *Nano Lett.* **11**, 5501 (2011)
10. M. Hocesvar, U.O. Krasovec, M. Berginc, G. Drazic, N. Hauptman, M. Topic, *J. Sol-Gel. Sci. Technol.* **48**, 384 (2008)
11. J. Jiu, S. Isoda, M. Adachi, H. Wang, *J. Mater. Sci. Mater. Electron.* **18**, 593 (2007)
12. H. Ellis, I. Schmidt, A. Hagfeldt, G. Wittstock, G. Boschloo, *J. Phys. Chem. C* **119**, 21775 (2015)
13. S. Zhang, Z. Lan, J. Wu, X. Chen, C. Zhang, *J. Alloys Compd.* **656**, 253 (2016)
14. A. Pandikumar, S.-P. Lim, S. Jayabal, N.M. Huang, H.N. Lim, R. Ramaraj, *Renew. Sustain. Energy Rev.* **60**, 408 (2016)
15. J.-K. Lee, B.-H. Jeong, S.-I. Jang, Y.-S. Yeo, S.-H. Park, J.-U. Kim, Y.-G. Kim, Y.-W. Jang, M.-R. Kim, *J. Mater. Sci. Mater. Electron.* **20**, 446 (2009)
16. S. Luo, H. Shen, Y. Zhang, J. Li, D. Oron, H. Lin, *Electrochem. Acta* **191**, 16 (2016)
17. K. Sodeyama, M. Sumita, C. O'Rourke, U. Terranova, A. Islam, L. Han, D.R. Bowler, Y. Tateyama, *J. Phys. Chem. Lett.* **3**, 472 (2012)
18. Z.-S. Wang, K. Sayama, H. Sugihara, *J. Phys. Chem. B* **109**, 22449 (2005)

19. V. Venkatraman, S. Abburu, B.K. Alsberg, *Phys. Chem. Chem. Phys.* **17**, 27672 (2015)
20. K. Hara, M. Kurashige, Y. Dan-oh, C. Kasasa, Y. Ohga, A. Shinpo, S. Suga, K. Sayama, H. Arakawa, *N. J. Chem.* **27**, 783 (2003)
21. H. Jia, H. Xu, Y. Hu, Y. Tang, L. Zhang, *Electrochem. Comm.* **9**, 354 (2007)
22. N. Fuke, L.B. Hoch, A.Y. Kopolov, V.W. Manner, D.J. Werder, A. Fukui, N. Koide, H. Katayama, M. Sykora, *ACS Nano* **4**, 6377 (2010)
23. A. Badawi, N. Al-Hosiny, S. Abdallah, S. Negm, H. Talaat, *Sol. Energy* **88**, 137 (2013)
24. A. Trenczek-Zajac, A. Kusior, A. Lacz, M. Radecka, K. Zakrzewska, *Mater. Res. Bull.* **60**, 28 (2014)
25. W. Li, J. Yang, Q. Jiang, Y. Luo, Y. Hou, S. Zhou, Y. Xiao, L. Fu, Z. Zhou, *J. Power Source* **307**, 690 (2016)
26. A. Jana, C. Bhattacharya, J. Datta, *Electrochim. Acta* **55**, 6553 (2010)
27. B. Sankapal, A. Tirpude, S. Majumder, P. Baviskar, *J. Alloys Compd.* **651**, 399 (2015)
28. M. Sabet, M. Salavati-Niasari, *Electrochim. Acta* **169**, 168 (2015)
29. G. Wang, S. Kuang, J. Zhang, S. Hou, S. Nian, *Electrochim. Acta* **187**, 243 (2016)
30. A. Chaves, K.S. Katiyan, S.P.S. Porto, *Phys. Rev.* **10**, 3522 (1974)
31. H.C. Choi, Y.M. Jung, S.B. Kim, *Vib. Spectrosc.* **37**, 33 (2005)
32. M. Abdulkbadar, B. Thomas, *Nano Struct. Mater.* **5**, 289 (1995)
33. H.G. Yang, G. Liu, S.Z. Qiao, C.H. Sun, Y.G. Jin, S.C. Smith, J. Zou, H.M. Cheng, G.Q. Lu, *J. Am. Chem. Soc.* **131**, 4078 (2009)
34. J.F. Dewald, in *Semiconductors*, ed. by N.B. Hannay (Reinhold, New York, 1959)
35. F. Fabregat-Santiago, J. Bisquerta, G. Garcia-Belmonte, G. Boschloo, A. Hagfeldt, *Sol. Energy Mater. Sol. Cell* **87**, 117 (2005)
36. Y. Tachibana, K. Umekita, Y. Otsuka, S. Kuwabata, *J. Phys. Chem. C* **113**, 6852 (2009)
37. R.Y. Yang, H.Y. Chen, F.D. Lai, *Adv. Mater. Sci. Eng.* **2012**, 1 (2012)
38. H. Li, C. Xie, Y. Liao, Y. Liu, Z. Zou, J. Wu, *J. Alloys Compd.* **569**, 88 (2013)
39. B.N. Mongal, S. Bhattacharya, S. Sengupta, T.K. Mandal, J. Datta, S. Naskar, *Sol. Energy* **134**, 107 (2016)